



1 **Partitioning snowmelt and rainfall in the critical zone: effects of**
2 **climate type and soil properties**

3
4 John C. Hammond^a, Adrian A. Harpold^b, Sydney Weiss^c, Stephanie K. Kampf^a

5
6 ^a Department of Ecosystem Science and Sustainability, Colorado State University, Fort Collins, CO 80523

7 ^b Department of Natural Resources and Environmental Science, University of Nevada, Reno, NV 89557

8 ^c College of Earth, Ocean, and Atmospheric Science, Oregon State University, Corvallis, OR 97331

9 *Correspondence to:* John Christopher Hammond (john.christopher.hammond@gmail.com)

10 **Abstract**

11
12 Streamflow generation and deep groundwater recharge in high elevation and high latitude locations may be
13 vulnerable to loss of snow, making it important to quantify how snowmelt is partitioned between soil storage, deep
14 drainage, evapotranspiration, and runoff. Based on previous findings, we hypothesize that snowmelt produces
15 greater streamflow and deep drainage than rainfall and that this effect is greatest in dry climates. To test this
16 hypothesis we examine how snowmelt and rainfall partitioning vary with climate and soil properties using a
17 physically based variably saturated subsurface flow model, HYDRUS-1D. To represent climate variability we use
18 historical inputs from five SNOTEL sites in each of three mountain regions with humid to semiarid climates:
19 Northern Cascades, Sierra Nevada, and Uinta. Each input scenario is run with three soil profiles of varying hydraulic
20 conductivity, soil texture, and bulk density. We also create artificial input scenarios to test how the concentration of
21 input in time, conversion of snow to rain input, and soil profile depth affect partitioning of input into deep drainage
22 and runoff. Results indicate that event-scale runoff is higher for snowmelt than for rainfall due to higher antecedent
23 moisture and input rates in both wet and dry climates. At the annual scale, surface runoff also increases with
24 snowmelt fraction, whereas deep drainage is not correlated with snowmelt fraction. Deep drainage is less affected by
25 changes from snowmelt to rainfall because it is controlled by deep soil moisture changes over longer time scales.
26 However, extreme scenarios with input highly concentrated in time, such as during melt of a deep snowpack, yield
27 greater deep drainage below the root zone than intermittent input. Soil texture modifies daily wetting and drying
28 patterns but has limited effect on annual scale partitioning of rain and snowmelt, whereas increases in soil depth
29 decrease runoff and increase deep drainage. Overall these results indicate that runoff may be substantially reduced
30 with seasonal snowpack decline in all climates. These mechanisms help explain recent observations of streamflow
31 sensitivity to changing snowpack and emphasize the need to develop strategies to mitigate impacts of reduced
32 streamflow generation in places most at risk for shifts from snow to rain.

33

34

35

36

37



38 1 Introduction

39

40 Snowmelt is the dominant source of streamflow generation and groundwater recharge in many high elevation and
41 high latitude locations (Regonda et al. 2005; Stewart et al. 2005; Earman et al., 2006; Clow, 2010; Jefferson, 2011;
42 Furey et al., 2012). Soils modulate the partitioning of snowmelt into subsurface storage, deep drainage, evaporative
43 losses and surface runoff. Snow persistence shows declines around the globe (Hammond et al., 2018b), and these
44 snow losses may lead to changes in water input magnitude and timing (Harpold et al., 2015; Harpold et al., 2017).
45 As areas of “at risk snow” become more apparent (Nolin and Daly, 2006), there is an urgent need for mechanistic
46 studies that quantify the partitioning of snowmelt in the critical zone among vapor losses, surface flow, and
47 subsurface flow and storage (Brooks et al., 2015; Meixner et al., 2016).

48

49 Changes in precipitation phase from snow to rain can modify hydrological partitioning by altering the timing and
50 rate of inputs. Snowmelt rates may not reach the extreme intensities of rainfall (Yan et al., 2018), but unlike rainfall,
51 which is typically episodic, snow can accumulate over time, then melting as a concentrated aggregate of soil water
52 input (Loik et al., 2004). Such concentrated snowmelt events can lead to a large proportion of runoff and deep
53 drainage (Earman et al., 2006; Berghuijs et al., 2014; Li et al., 2017). With climate warming, future snowmelt rates
54 may be reduced in many areas because earlier melt occurs when solar radiation is lower (Musselman et al., 2017).
55 Along with warmer temperatures, increasing atmospheric humidity is leading to more frequent and greater
56 magnitude mid-winter melt events in humid regions, and increased snowpack sublimation and/or evaporation in dry
57 regions (Harpold and Brooks, 2018). Some areas (i.e. the Cascades) are predicted to receive more intense water
58 inputs with rainier futures, whereas others (i.e. Southern Rockies) will likely experience declines in input intensity
59 with snow loss (Harpold and Kohler, 2017). Given the considerable heterogeneity in the factors that affect
60 hydrological partitioning, such as climate, soils, topography, and vegetation, different locations may not respond in
61 the same way to loss of snow.

62

63 Water inputs from rain or snowmelt during periods of low potential evapotranspiration and higher antecedent
64 moisture conditions are more likely to generate runoff and deep drainage (Molotch et al., 2009). Prior research has
65 shown that near-surface soil moisture response is closely related to snow disappearance (Harpold and Molotch,
66 2015; Webb et al., 2015; Harpold et al., 2015) with strong links between snowmelt and soil moisture dynamics at
67 multiple spatial and temporal scales (Loik et al. 2004; Williams et al. 2009; Blankinship et al. 2014; Kormos et al.,
68 2014; Harpold and Molotch, 2015; Webb et al. 2015; Kampf et al. 2015). Earlier snow disappearance can lead to
69 lower average soil moisture conditions not as conducive to streamflow generation as later snowmelt (Kampf et al.
70 2015). The effects of earlier snowmelt on soil moisture dynamics may also vary with precipitation after snowmelt.
71 Late-spring precipitation can overwrite the signal of earlier snowmelt timing on spring and summer soil moisture
72 (Liator et al., 2008, Conner et al., 2016), whereas a lack of spring and summer precipitation can cause effects of
73 earlier snowmelt on soil moisture to persist longer (Blankinship et al, 2014; Harpold, 2016). Earlier snow
74 disappearance can lead to diverging patterns in growing season length; a longer growing season if energy hinders



75 vegetation growth, or a shorter growing season when soil water stress limits productivity (Harpold et al., 2015;
76 Harpold, 2016; Hu et al., 2010).
77
78 Both runoff and deep drainage are affected by soil texture, soil depth, rooting depth (Cho and Olivera, 2009;
79 Seyfried et al., 2005) and topography. These properties have limited variability over timespans of hydrologic
80 analysis and can produce temporally stable spatial patterns of soil moisture, where some parts of the landscape are
81 consistently wetter than others (Williams et al., 2009; Kaiser and McGlynn, 2018). Aspect modifies the snowpack
82 energy balance, leading to higher sustained moisture content on north-facing slopes compared to south-facing slopes
83 with the same input (in the northern hemisphere); landscape evolution due to wetter conditions on north-facing
84 slopes may lead to deeper profiles and more deeply weathered rock conducive to deep drainage in some locations
85 (Hinckley et al., 2014; Langston et al., 2015). Where soils are shallow, winter precipitation may exceed the soil
86 storage capacity, leading to both runoff generation and deep drainage (Smith et al., 2011). Deeper soil profiles have
87 greater storage capacity, which can sustain streamflow, even with snow loss; however, given consecutive years of
88 low input these profiles will be depleted of storage leading to lower flows (Markovich et al., 2016). Deeper soils can
89 also help sustain transpiration during the late spring and summer, when shallow soils have already dried (Foster et
90 al. 2016; Jepsen et al., 2016). Streamflow can be insensitive to inputs under dry conditions, but respond rapidly
91 once a threshold soil moisture storage value is exceeded (McNamara et al., 2005; Liu et al., 2008; Seyfried et al.,
92 2009). McNamara et al. (2005) hypothesized that when dry-soil barriers are breached, there is sudden connection to
93 upslope soils, leading to delivery of water to areas that were previously disconnected. In their semi-arid study area,
94 such breaching of dry-soil barriers was only observed for periods of concentrated and sustained input from high-
95 magnitude spring snowmelt. Together the complex interactions of soil properties, antecedent conditions, water
96 inputs, and evaporative demand make it challenging to determine how changes from snow to rain affect hydrologic
97 response even in idealized settings.

98
99 The goal of this study is to improve our understanding of how changes in precipitation phase from snow to rain
100 affect hydrological partitioning in a one-dimensional (1-D) representation of the critical zone. Partitioning of
101 precipitation input, P , can be into runoff, Q , defined as lateral export of water from the domain; evaporation, E ;
102 transpiration, T ; deep drainage below the root zone, D ; and storage within the soil root zone, ΔS . Over a given time
103 increment, partitioning can be tracked using the water balance (equation 1).

104

$$105 \quad P = Q + E + T + D + \Delta S \quad (1)$$

106

107 We address the questions: (1) Are snowmelt and rain partitioned differently between Q , E , T , and D ? and (2) How is
108 snowmelt and rain partitioning affected by climate, soil type, and soil depth? We use a physically-based 1-D
109 modeling approach to address these questions and systematically test hypotheses about hydrologic response to snow
110 loss.

111



112 We hypothesize that reducing the fraction of precipitation falling as snow leads to lower runoff and deep drainage
113 because it reduces the concentration of input in time (Figure 1). Concentrated input during melt of a seasonal
114 snowpack often saturates soils, causing saturation excess runoff and deep drainage below the root zone (Hunsaker et
115 al., 2012; Kampf et al., 2015; Webb et al., 2015; Barnhart et al., 2016). Diffuse input over time reduces the
116 likelihood of saturation because it allows time for water redistribution and evapotranspiration between inputs. We
117 also hypothesize that snowmelt is critical for runoff generation and deep drainage in dry climates and deep soils,
118 where snowmelt is the dominant cause of soil saturation (McNamara et al., 2005; Tague and Peng, 2013), whereas
119 the partitioning of rain and snowmelt may be more similar in wet climates and shallow soils, which are more
120 frequently saturated by either rain or snowmelt inputs (Loik et al., 2004) (Figure 1).

121

122 **2 Methods**

123

124 To evaluate soil moisture response to rainfall and snowmelt over a wide range of climate and soil conditions we
125 used HYDRUS-1D (Šimůnek et al. 1998), a physically-based finite element numerical model for simulating one-
126 dimensional water movement in variably saturated, multi-layer, porous media.

127

128 **2.1 Study design, site selection, and data sources**

129

130 We utilized daily input data from five United States Department of Agriculture Natural Resources Conservation
131 Service (NRCS) snow telemetry (SNOTEL) sites in each of three regions that span a wide range of climate and
132 snow conditions: the Cascades, Sierra Nevada, and Uinta mountains for a total of 15 sites. Daily rather than hourly
133 data were chosen to limit the effects of missing and incorrect values on the analyses. The three regions chosen to
134 represent dominant climate types in the western U.S., and within each region, sites were selected to span a snow
135 persistence (SP) gradient, which is the mean annual fraction of time that an area is snow covered between Jan 1 and
136 Jul 3 (Moore et al., 2015) over the ~35 years of record (Figure 2a, Table 1).

137

138 With each climate scenario we simulated vertical profiles of volumetric water content (VWC), which were depth-
139 integrated to compute soil moisture storage (S). For these simulations deep drainage (D) is any flux of water
140 downward below the root zone. Runoff (Q) is any water that does not infiltrate into the soil, either because of
141 saturated conditions or because input rates exceed infiltration capacity. Evaporation (E) is direct evaporation from
142 the soil, and transpiration (T) is mediated by plant roots; for this study, these values are combined into
143 evapotranspiration (ET) to represent the bulk loss of water to the atmosphere.

144 Daily precipitation (P), snow water equivalent (SWE), and volumetric water content (VWC) at 5, 20, and 50 cm
145 were obtained for each SNOTEL site using the NRCS National Weather and Climate Center (NWCC, 2016) Report
146 Generator (Table 1). The records were quality controlled to ensure reasonable precipitation, SWE and VWC values
147 as in Harpold and Molotch (2015). Unrealistic values were removed (i.e. negative SWE, VWC below zero or above
148 unity); all daily VWC outside of three standard deviations from the mean were removed, and a manual screening



149 was performed on VWC data to identify shifts and other artifacts not captured by the first two automated
150 procedures. Daily potential evapotranspiration (PET) was extracted from daily gridMET (Abatzoglou, 2013) for the
151 4 km pixel containing each SNOTEL site. This product uses the ASCE Penman-Monteith method to compute PET.

152

153 We chose three SNOTEL sites (432 Carrant Creek, 698 Pole Creek R.S., 979 Van Wyck) to represent soil profile
154 characteristics. While 365 of the 747 SNOTEL sites in the western U.S. have soil moisture sensors, only a fraction
155 of these sites have detailed soil profile data. The sites with soil profile data have information obtained from soil
156 samples taken in the soil pits and processed in the NRCS Soil Survey Laboratory in Lincoln, NE for texture, water
157 retention properties, and hydraulic conductivity. We obtained detailed soil profile data, in the form of pedon primary
158 characterization files from the NRCS, and selected three profiles (Figure 2b, Table 2) that represent the range of soil
159 textures and hydraulic conductivity values present at SNOTEL locations. Each had detailed NRCS pedon primary
160 characterizations to depths greater than 100 cm and >15 years of daily soil moisture records at 5, 20 and 50 cm
161 depths.

162 **2.2 Simulations**

163

164 In HYDRUS-1D, we simulated water flow and root water uptake for a vertical domain 10 m deep. The domain was
165 discretized into 500 nodes with higher node density near the surface (~0.15 cm for top 5 cm to ~5 cm for the bottom
166 of the profile). For the surface boundary, we used a time variable atmospheric boundary condition, which allows
167 specifying input (snowmelt and rain) and potential evapotranspiration (PET) time series. Runoff can also be
168 generated at the surface boundary. For the lower boundary, we allowed free drainage from the bottom of the soil
169 profile at 10 m. Surface soil water input was calculated by totaling snowmelt and rainfall input at the daily time step
170 from SNOTEL precipitation and SWE values. Melt was computed for any day when SWE decreased; if SWE
171 decreased, and the precipitation was greater than 0, total soil water input was assumed to be melt plus precipitation.
172 The atmospheric boundary condition requires PET, leaf area index (LAI), and a radiation extinction coefficient used
173 in the estimation and separation of potential evaporation and transpiration. We assigned a constant LAI of three, as
174 this value generally fits the mixed conifer forests (Jensen et al., 2011) where SNOTEL sites are installed and
175 assumed a radiative extinction coefficient of 0.39, which is the default value. Root water uptake in the model was
176 estimated using Feddes parameters for a conifer forest (Lv, 2014: h_1 0 cm, h_2 0 cm, h_{3h} -5,100 cm, h_{3l} -12,800 cm,
177 h_4 -21,500 cm, $T_{P_{low}}$ 0.5 cm/d, $T_{P_{high}}$ 0.1 cm/d), with roots uniformly distributed from the soil surface to the
178 interface with a lower hydraulic conductivity layer, as we lacked any more detailed information on root distribution
179 or soil depth at these sites.

180

181 We created soil layers with depths and textures taken from the NRCS soil pedon measurements. From this
182 information we applied the neural network capability of HYDRUS-1D, which draws from the USDA ROSETTA
183 pedotransfer function model (Schaap et al., 2001), to determine soil hydraulic parameters. Using the NRCS pedon
184 primary characterizations we input percent sand, silt and clay, bulk density, wilting point, and field capacity; the
185 neural network model estimates soil hydraulic parameters based on these inputs. Below the depth of the soil pedon



186 measurements, we configured the simulations to have a deep “bedrock” or regolith layer with lower saturated
187 hydraulic conductivity (K_s) but the same water retention parameters as the layer above. Any water entering this
188 lower layer is considered deep drainage. The hydraulic conductivity of this lower layer was set at one tenth that of
189 the layer above; this value was determined through iterative testing of K_s values (see Supplementary). We extended
190 the “bedrock” or regolith layer to 10 m depth to allow for deep drainage to occur without boundary effects that could
191 be caused by a shallower regolith. The initial VWC for all layers in each simulation was 0.2, and simulations were
192 run with a year of surface boundary condition inputs to establish initial conditions. We tested the simulation
193 configuration by comparing to observed VWC at 5, 20 and 50 cm depths for the three selected soil profile sites
194 (Figure S1, Table S1). Rather than force-fitting, our goal was to produce simulations with similar timing of wetting
195 and drying to observations. This approach is consistent with other studies using HYDRUS – 1D, which also started
196 with basic soils data and application of the ROSETTA pedotransfer function (Scott et al., 2000) and then calibrated
197 to observed water content measurements by adjusting permeability of the “bedrock” layer (Flint et al., 2008).

198

199 We applied climate scenarios from each of the 15 SNOTEL sites selected (Table 1) to each of the soil profiles to
200 examine how climate and soil type affect partitioning. We then conducted additional experiments to modify inputs
201 using just the loam profile. First to examine whether snowmelt and rainfall are partitioned differently, we changed
202 all precipitation to rain and compared the simulation output to those with the original climate data. Second, to
203 examine the effects of input concentration, we artificially produced intermittent input (four five-day periods of low
204 magnitude) and concentrated input (one twenty-day period of high magnitude) of the same annual total for one wet
205 (559) and one dry (375) site using the loam profile (1056) for all years of data. Third, to examine how soil depth
206 affects partitioning we altered the depth of rooting zones to 0.5, 1.5 and 2 times their original depth. For 0.5 depth
207 scenarios, we replaced soil layers deeper than 0.5 times the original depth with the bedrock/regolith layer. For 1.5x
208 and 2x scenarios, the layer above bedrock/regolith was extended downward, and the rooting zone extended to the
209 new soil depth.

210

211 **2.3 Analysis**

212

213 Using the simulation results, we examined how rain and snowmelt were partitioned into soil storage (S), deep
214 drainage (D), evapotranspiration (ET), and runoff (Q). Daily soil storage is reported as the total soil water within the
215 rooting zone only, and D is any water passing below the rooting zone (106-127 cm depending on the soil profile).
216 We assessed partition components both in units of length (cm) and as ratios to total input (unitless, e.g. Q/P) at both
217 event and annual time scales.

218

219 To analyze hydrologic partitioning at event time scale we defined rainfall events as days with precipitation while
220 SWE equaled zero and snowmelt events for days with declining SWE and no simultaneous precipitation. To focus
221 on differences between rainfall and snowmelt, only events with entirely rainfall or entirely snowmelt input were
222 considered in this analysis; mixed events were excluded. Events could last as long as the conditions were



223 continuously satisfied, and only those followed by at least five days of no input were used in analysis. Total depths
224 of each variable were computed for each defined event time period; input rain and snowmelt were summed over the
225 event time period, and response variables (Q, ET, D) also included the day after the event ended to account for lag in
226 event response. Antecedent S for each event was determined by taking the root zone storage from the day prior to
227 the first event input.

228

229 At the annual scale, soil water input and partitioning components (rain, snowmelt, Q, ET, D) were totaled for each
230 year, and the change in water year storage (ΔS) determined by subtracting the values of S at the end of the year from
231 the value at the beginning of the year. In addition to ΔS , mean saturation (Sat) at each observed depth was calculated
232 as the average annual VWC divided by soil porosity. We use mean saturation (Sat) as an alternative to change in
233 water year storage (ΔS) because mean saturation is much easier to quantify at a field site than root zone storage, and
234 this extends the application of our study to other areas with daily VWC data. Sat also provides a measure of soil
235 water conditions throughout the year as opposed to ΔS which represents only changes between the start and end of
236 the water year.

237

238 To characterize climate conditions at the mean annual scale, each site was classified as dry (precipitation deficit,
239 $PET > P$) and wet (precipitation surplus, $PET < P$). This separation by aridity index is based on our hypothesis that the
240 influence of concentrated snowmelt is greater in dry climates than in wet climates (Hammond et al, 2018a). We also
241 report the maximum SWE and snowmelt fraction as the annual total snowmelt divided by annual total input.
242 Following the methods for computing the precipitation concentration index (PCI), which represents the continuity or
243 discrete nature of input through time (Martin-Vide, 2004; Raziei et al., 2008; Li et al., 2011), we computed the input
244 concentration index (ICI) using snowmelt and rain input. Pearson correlation tests were conducted between
245 explanatory variables (P, PET, P/PET, peak SWE, average melt rate, and ICI) and dependent variables (Q, ET, D,
246 mean saturation at 100 cm: Sat100).

247

248 Using both the event and annual results, we examined (1) whether partitioning of rainfall input differed from that of
249 snowmelt input, and (2) how partitioning was affected by climate, soil texture, and soil depth. For question 1, we
250 tested for differences in event partitioning between input type (rain or snowmelt) and differences in annual
251 partitioning between historical and all rain scenarios using ANOVA. For question 2, we tested for differences in
252 annual partitioning between climate (wet, dry) and soil depth groupings, also using ANOVA. Additionally for
253 question 2, we tested the pairwise difference in linear regression slopes using indicator-variable regression with
254 interaction in JMP (SAS-based statistical software) to determine whether the rate of change between explanatory
255 and response variable differed by climate or soil depth grouping.

256

257

258

259



260 3 Results

261

262 Simulations for each of the 15 climate scenarios exhibit substantial variability at the annual scale in precipitation
263 (P), runoff (Q), and deep drainage (D) (Figure 3). All regions have a wide range of annual P, but overall the highest
264 P was in the Cascades region and lowest in the Uinta. The wide range of climate conditions simulated allows for an
265 evaluation of climate effects on Q, ET, D, and Sat100 (Table S3). Annual precipitation (P) is positively correlated
266 with runoff (Q, $r=0.97$), deep drainage (D, $r=0.92$), and Sat100 ($r=0.73$) (Table S3). The relationship is linear for Q
267 but nonlinear for D and Sat100. Sat100 plateaus at ~250 cm P with further P partitioned to Q instead of D.
268 Evapotranspiration (ET) has the weakest correlations with P ($r=0.08$) of all partitioned components. Q/P increases
269 with P up to around 250 cm of P, and D/P increases with P up to around 100 cm (Figure 3). ET/P decreases with
270 precipitation, whereas S/P is unrelated to P. At values of P greater than around 300 cm, all variables have relatively
271 consistent values even as P increases.

272

273 3.1 Snowmelt vs rainfall and climatic influences on partitioning

274

275 Our first research question asks whether snowmelt and rainfall are partitioned differently. At the event scale, input
276 rates are significantly greater on average for snowmelt than for rainfall in each of the three regions and for the full
277 dataset (ANOVA $p<0.0001$, mean snowmelt 1.1 cm/d, mean rainfall 0.9 cm/d, Figure 4), though rainfall events have
278 a higher maximum input rate (maximum snowmelt 8.0 cm/d, maximum rainfall 14.7 cm/d). Snowmelt events tend to
279 occur on wetter soils, as estimated by antecedent soil moisture storage for the rooting zone (ANOVA $p<0.0001$,
280 mean S for snowmelt 56.6 cm, mean S for rainfall 48.2 cm). Average runoff ratios (Q/P) are higher for snowmelt
281 than for rainfall (ANOVA $p<0.0001$, mean Q/P snowmelt 0.20, mean Q/P rainfall 0.03), whereas ET/P is lower for
282 snowmelt as compared to rainfall (mean snowmelt 0.24, mean rainfall 0.40). Deep drainage responses are affected
283 by longer time scales than single events, so we did not include these in the event analysis.

284

285 At the annual scale, input at all sites is a mixture of rain and snowmelt. To examine the importance of snow to
286 partitioning, we used snowmelt fraction, defined as the fraction of snowmelt to total precipitation, and input
287 concentration index (ICI). Snowmelt fraction and snow persistence are generally positively correlated with ICI at
288 dry sites in the Uinta and Sierra, but this correlation declines with wetter sites in the Cascades (Figure S7). This
289 indicates that areas with greater snowmelt tend to have greater input concentration in dry climates. Q/P increases
290 with snowmelt fraction ($r=0.41$), most noticeably where snowmelt fraction is >0.5 and increases with ICI ($r=0.80$)
291 (Figure 5). The ranges of Q/P are higher in wet than in dry climates, though dry climates show greater rates of
292 change with increasing snowmelt fraction and input concentration (Table S4). D/P is somewhat correlated with
293 snowmelt fraction ($r=0.20$) and ICI ($r=0.43$). D/P ranges are higher in wet than in dry climates, with many dry years
294 not generating D. ET/P is not related to snowmelt fraction and generally declines with ICI ($r = -0.75$); ranges are
295 lower for wet climates, where greater input is partitioned to Q and D.

296



297 We then compared the hypothetical scenarios where we treated all precipitation as rain to snow-dominated historical
298 scenarios. All rain leads to significantly lower Q/P ($p < 0.0001$, all rain mean 0.17; historical mean 0.31) for both wet
299 and dry sites (Table 3, Figure 6). This partly relates to lower near-surface saturation in all rain scenarios; the mean
300 fraction of annual runoff from saturation excess is 88% when all input is rain as compared to 97% with historical
301 rain and snow input. All rain also leads to higher ET/P for dry sites ($p < 0.0001$, all rain mean 0.95; historical mean
302 0.83); lower D/P for dry sites (all rain mean 0.01; historical mean 0.03), and higher D/P at wet sites ($p = 0.011$, all
303 rain mean 0.14; historical mean 0.12) (Table 3, Figure 6).

304

305 Another effect of snow loss can be a decrease in input concentration because snow melt concentrates input in a short
306 period of time. Experimental scenarios with constant P separated into intermittent and concentrated inputs for a wet
307 site (375) and a dry site (559) show that increasing input concentration leads to significantly greater Q/P in the dry
308 site ($p < 0.05$, intermittent mean 0.54, concentrated mean 0.68, Table 3, Figure 6) but no significant difference in the
309 wet site. In contrast, D/P is significantly greater ($p < 0.0001$) for the concentrated input scenarios for both dry and
310 wet sites, as no deep drainage is produced with intermittent input. ET/P is significantly lower in concentrated input
311 scenarios, with a greater difference in dry climates ($p = 0.004$, mean intermittent 0.80 vs. concentrated 0.66) than in
312 wet climates ($p = 0.013$, mean intermittent 0.34 vs. concentrated 0.28).

313

314 **3.2 Soil property influences on partitioning**

315

316 Soil stores water that may later be partitioned into Q, ET, and D. Using Sat100 as an indicator of soil moisture
317 storage, Figure 7 displays the relationships between Q/P, D/P and ET/P vs Sat100 as separated by climate type, soil
318 texture, and root zone depth. Sat100 has strong relationships with Q/P, D/P, and ET/P for all, wet, and dry sites
319 (Figure 7, Table S5). Q/P is generally low (Figure 7a, < 0.3) until Sat100 is greater than > 0.5 . D/P in the simulations
320 also increases with Sat100, and many simulation years have limited D when Sat100 < 0.5 . ET/P generally decreases
321 with saturation for Sat100 values > 0.5 .

322

323 When these same relationships are separated by soil texture rather than wet/dry climate (Figure 7b, Table S5), the
324 response patterns are similar between soil types except for the sandy loam profile, which displays higher Q/P and
325 D/P than the loam and sandy clay loam profiles at similar Sat100 levels. Differences between responses by soil
326 texture are more evident at sub-annual time scales (Figure 8a). For the example time period shown in Figure 8a,
327 loam and sandy clay loam profiles wet up each spring during snowmelt prior to the sandy loam profile, and their
328 higher water retention means they can generate deep drainage earlier and longer than sandy loam. However, sandy
329 loam has higher K_s , which allows a greater rate of deep drainage during time periods of saturation. Consequently,
330 the differences in deep drainage between soil textures are limited (Figure 6), except that annual D/P for sandy loam
331 is higher than for sandy clay loam and loam profiles when Sat100 values are low. The latter soils retain more water,
332 so they ultimately reach the highest annual D/P values at higher Sat100 values. More water retention in the sandy
333 clay loam and loam soils can lead to more runoff generation via saturation excess, whereas the drier conditions in



334 sandy loam can lead to infiltration excess runoff. However, the net differences in annual total runoff are limited
335 between the three soil textures (Figure 6).
336 To assess the influence of soil profile depths on partitioning, we altered the loam soil profile to be 0.5x, 1.5x and 2x
337 times its original depth (Figure 6, Table 3). For historical input, Q/P and D/P are greatest for the 0.5x depth scenario,
338 and Q/P declines significantly with deeper soils for both dry and wet sites ($p < 0.0001$), with the greatest declines
339 between 0.5x and 1x (original) depth. D/P declines significantly between 0.5x and 1x depth, then increases slightly
340 for all sites with subsequent increases in depth to 1.5x and 2x (Figure 6, Table 3). Q/P and D/P differences by depth
341 are significant between 0.5x and 1x depth, but not for all subsequent depth comparisons for all, wet and dry site
342 classifications (Table 3). In pairwise comparisons between depth scenarios Q/P is only significantly different
343 between 0.5x and 1x depth categories ($p < 0.0001$). Changes in ET/P with soil depth are not significant according to
344 ANOVA tests.

345
346 Figure 8b displays daily time series of surface runoff, deep saturation, deep drainage, and cumulative deep drainage
347 during an example period for the four different soil root zone depth scenarios. The shallowest rooting zone of 0.5x
348 original depth displays the greatest surface runoff as well as cumulative deep drainage throughout the example
349 period. Each depth reaches and remains at saturation for different amounts of time, with the shallowest profile
350 reaching saturation earliest and remaining saturated longest, but also decreasing more rapidly to the lowest ending
351 saturation. The deepest profile takes the longest to increase Sat100, not reaching as high a peak, yet remaining
352 higher at the end of the period. Deep drainage occurs earliest for the shallowest depth scenario, though reaching a
353 lower daily flux than the original depth. Deep drainage from the 1x 1.5x and 2x original depth scenarios lag behind
354 the 0.5x scenario following the same succession as their Sat100 patterns. These patterns in daily Sat100 and deep
355 drainage result in the highest cumulative deep drainage for the shallowest scenario.

356

357 **4 Discussion**

358

359 **4.1 Snowmelt as an efficient runoff generator and factors accentuating snowmelt efficiency**

360

361 The initial hypotheses for this study were that runoff and deep drainage would be greater from snowmelt than
362 rainfall. Multiple lines of evidence from our 1-D hydrologic simulations point towards snowmelt as a more efficient
363 driver of runoff, and to a lesser extent deep drainage, than rainfall. Results confirmed that runoff efficiency from
364 snowmelt events was elevated because snowmelt events were 22% greater in input rate, and occurred on 17% wetter
365 soils than rainfall. This stands in agreement with previous studies showing that snowpack development and
366 subsequent melt tend to occur when soils are at elevated moisture contents due to lower ET (Liu et al., 2008;
367 Williams et al., 2009; Bales et al., 2011). Whether input is snowmelt or rainfall becomes less important for
368 hydrologic response at annual times scales, for which the correlation between snowmelt fraction and response
369 variables is weak to moderate (Figure 5, Table S3). When input scenarios are forced into the extreme case of all rain,
370 they show a lower annual Q/P (Dry: 0.13 vs. 0.04; Wet: 0.46 vs. 0.29), corroborating the event results that indicate
371 snowmelt elevates runoff (Table 3, Figure 6). We also hypothesized that the effects of changing snowpacks would



372 be greatest in dry climates, where soil saturation is less frequent. However, evidence suggests that both wet and dry
373 climates are likely to show reduced surface runoff with declining snow water inputs at the 1-D scale.

374

375 We had hypothesized based on prior research (Hunsaker et al., 2012; Langston et al., 2015; Barnhart et al., 2016; Li
376 et al., 2017; Hammond et al., 2018a) that input concentration would be the primary reason for elevated Q and D
377 from snowmelt relative to rainfall. While ICI is correlated with increasing Q/P and D/P (Figure 5, Table S3),
378 snowmelt is not consistently the cause of greater input concentration in the wetter sites (Figure S7). When input is
379 extremely concentrated, as in the hypothetical experiments (Table 3, Figure 6) D/P increases significantly in both
380 wet and dry climates, whereas Q/P only increases significantly with input concentration in dry climates. Therefore,
381 snowmelt likely enhances runoff due to greater input concentration in dry climates, whereas the importance of snow
382 for concentrated input reduces with wetter climates, where greater runoff from snowmelt may relate more to higher
383 antecedent moisture.

384

385 The effects of snow loss on D were not as consistent across our simulations as the effects on Q. In general, Q/P was
386 greater than D/P, so Q was more sensitive to changes in input: Q was higher for snowmelt than rainfall events; Q/P
387 decreased in all rain simulations, increased in concentrated input simulations, and increased with both snowmelt
388 fraction and input concentration at the annual time scale. In contrast D/P increased for all rain simulations in wet
389 climates but decreased in dry, increased in concentrated input simulations, and was not strongly correlated to
390 snowmelt fraction. This variability in D/P response as compared to Q/P is likely because S mediates the connection
391 between input and D. In the 1D model Q is affected by infiltration rate and near-surface storage and can more
392 rapidly respond to input changes. In the simulations shown here once subsurface storage is at capacity, D will
393 plateau, and Q will increase with further input due to the saturation excess mechanism.

394

395 Soil texture and depth generally do not change partitioning at the annual time scale as much as the varying climate
396 scenarios (Figure 6), although both runoff and deep drainage increase in the shallowest soils. Shorter durations of
397 deep drainage for the coarser sandy loam profile compared to the finer texture soils are offset by higher rates of flux
398 during deep drainage in the coarser profile (Figure 8a). Lower likelihood of surface saturation in the sandy loam soil
399 compared to other soils is offset by greater likelihood of infiltration excess runoff. Altering soil profile depth and the
400 associated root zone to 0.5, 1.5x and 2x the original depth produces the largest effects on Q/P and D/P from 0.5x to
401 1x depth, and mixed directional response from 1x to 2x depth (Table 3, Figure 6). When soil depths exceed the 1x
402 scenario, the relative amounts of Q and D change (Figure 6). Q gradually declines with greater storage because
403 surface soils do not stay as wet, whereas D gradually increases with greater storage because less water is lost to Q.
404 The responsiveness of fluxes to changes in soil depth from 0.5-1x may relate to storage capacity relative to input.
405 The soil depths ranged from 106-127 cm, which with a porosity of 0.4 gives a storage capacity of 42-51 cm, large
406 enough to store the mean annual precipitation in most watersheds (Figure 3). When this storage is reduced by half to
407 21-25 cm, it is smaller than the mean annual precipitation at the wetter sites, which would lead to greater likelihood
408 of soil saturation that leads to D and Q. Consequently the change in profile depth from 0.5 m to 1 m represents a
409 shift from annual input greatly exceeding profile storage, to storage approximately accommodating annual input. At



410 the sites used in this study, mean annual P ranges from 0.8 to 11.3 times the storage of the 1x soil profile, and peak
411 SWE ranges from 0.1 to 5.9 times the storage. Reducing soil depth increases the likelihood that peak SWE will
412 exceed the soil storage capacity, leading to greater surface runoff and deep drainage (Smith et al., 2011). Deeper
413 rooting depths can allow more water to remain in storage and be lost to ET before contributing to surface runoff and
414 deep drainage (Smith et al., 2011).

415

416 **4.2 Uncertainties**

417

418 Given the complex nature of soil water movement in heterogeneous mountain topography, this study makes several
419 assumptions and simplifications. The simulations do not include the intricacies of vegetation water use, and the
420 routine chosen assumes a static leaf area index (LAI) with root uptake controlled only by PET and soil moisture.

421 The water balance in hydrologic models can be highly sensitive to the method chosen to represent root uptake and
422 plant water use (Gerten et al., 2004), and hydrologic models generally poorly capture or replicate the interactions
423 between soil, vegetation and atmospheric properties that combine to control plant water use (Gómez-Plaza et al.,
424 2001; Gerten et al., 2004; Zeng et al., 2005). Additionally, simulations are generally wetter than measured water
425 contents; therefore, the representation of partitioning shown here displays relative response between climates and
426 soil profiles rather than absolute quantification of these partitioned components.

427

428 Hydrologic response in hillslopes and catchments is not fully captured in the 1-D modelling approach. Sites across
429 elevation and precipitation gradients in this study show different responses within each region with generally lower
430 Q/P and D/P at drier, lower elevations (Figure S6). Within each elevation zone, local variability in microclimate,
431 vegetation, and soil properties can also lead to heterogeneity in input and partitioning. In addition, we did not allow
432 for frozen soils in our simulations, but this can be a strong influence on soil input partitioning in places where snow
433 depth was <50 cm and incapable of insulating the soil (Slater et al., 2017). The 1-D model does not incorporate
434 lateral surface or subsurface flow, which can be redistribute water downslope along the soil snow interface (Webb
435 et al., 2018) and within the shallow subsurface (Kampf et al., 2015). Lateral redistribution of water thus leads to
436 spatially variable patterns of input, storage, runoff generation, and ET at the hillslope to watershed scales (Brooks et
437 al., 2015). While simulating only vertical flow is reasonable for SNOTEL sites located in relatively flat forest
438 openings, 1-D simulations will tend to be biased wet because they do not allow any lateral redistribution. A
439 progression of the work shown here would be to simulate 3-D flow and examine the spatial variability in effects of
440 snow loss. For example, a decline in deep drainage near a ridge line, where flow paths are predominantly vertical
441 could reduce subsurface flow emergence at downslope locations, and this decreased groundwater emergence may
442 reduce ET in areas where vegetation is reliant on the emergence of deeper flow paths. Water partitioned into Q and
443 D in a 1-D model may not represent the same Q and D observed at a stream: Q generated at a point location may
444 infiltrate downslope; D may also emerge downslope to supply streamflow rather than remaining in the deep
445 subsurface.

446



447 The partitioning of input into the components used here (Q,D,ET,S) is affected by soil depth. The profile depths we
448 simulated represent the minimum likely soil depth, as the collection of the pedon reports was limited by the depth of
449 refusal for sample collection. Shallow soil profiles can also lead to a wet bias in simulations, and this can artificially
450 elevate saturation excess flow leading to our observations of greater Q/P than D/P in most site-years. Saturation
451 excess overland flow has been documented in the elevation bands of many SNOTEL sites (Newman et al., 2004;
452 Eiriksson et al., 2013; Kampf et al., 2015), but it may not occur as frequently as simulated.

453
454 Sub-daily dynamics in snow melt and ET are not captured by our use of a daily time step. We chose to model soil
455 water response to rainfall and snowmelt at the daily timestep due to better data quality, but processes affecting
456 partitioning of these inputs take place at sub-daily scales. Comparisons of results from simulations using daily vs
457 hourly input demonstrate similar timing of response, but greater cumulative surface runoff from hourly simulations
458 and greater cumulative deep drainage from daily simulations (Table S2, Figure S2). The short hourly time period
459 allows for higher intensity input, which causes infiltration excess overland flow, whereas daily input is of lower
460 intensity, allowing for greater deep percolation.

461
462 The simulations used here only allow for matrix flow, excluding macropore flow, for a simplified representation of
463 soil water movement. Preferential flow though the profile can enhance deep drainage relative to surface runoff,
464 which is another potential reason why soil moisture simulations were biased wet. 60-80% of deep drainage has been
465 shown to occur as preferential rather than interstitial flow (Wood et al., 1997; Jaynes et al., 2001; Sukhija et al.,
466 2003), yet our dry climate simulated annual D/P of ~0.05 is of similar magnitude to that reported prior (Wood et al.,
467 1997). The simulated Q/P (~0.0-0.9) vs snowmelt fraction plots from HYDRUS-1D simulations follow the same
468 general increasing pattern ($r = 0.41$) as Q/P (~0.0-1.0) vs SP in Hammond et al., 2018a ($r = 0.39$). This lends
469 confidence to the HYDRUS-1D simulations, as their simulated values are in the same range as observed streamflow.

470

471 **5 Conclusions**

472

473 This study helps to explain the mechanisms that lead to greater runoff from snowmelt. At event scale snowmelt
474 generates more runoff because it tends to be greater in input rate and to occur on wetter soils than rainfall; the
475 concentration of input during seasonal snowmelt elevates runoff in dry climates but has less of an influence as in wet
476 climates. Deep drainage can also decline with loss of snow, but it has a weaker response because soil storage buffers
477 the impacts of snow loss. Soil texture modifies short-term timing of soil moisture and runoff generation, but these
478 effects are not large enough to alter the annual response of different soil types to changes in snow. Soil depth can
479 have a greater effect on input partitioning, particularly where soil water storage is less than mean annual
480 precipitation. Soils that are shallower than observed soil depths generate the greatest runoff and deep drainage,
481 indicating that shallow soils may show the largest changes in partitioning as input transitions from snowmelt to
482 rainfall. Increasing soil depth above observed depths gradually reduces surface runoff while increasing deep
483 drainage. The 1-D simulations provide basic hypotheses for hydrologic partitioning under changing snowmelt that



484 should be further explored in a 2-D or 3-D hydrological models and direct observations. Although more work is
485 necessary to translate these finding to streamflow response, water managers should develop strategies to mitigate
486 impacts of reduced streamflow generation in places that are most at risk for shifts from snow to rain.

487

488 **Author Contributions**

489

490 JH, AH and SK designed the experiments and JH and SW carried them out. JH and SW performed the simulations.
491 JH conducted statistical analyses on model outputs. JH prepared the manuscript with contributions from all co-
492 authors.

4931. **Competing interests**

494 The authors declare that they have no conflict of interest.

495 **Acknowledgements**

496 This research was supported by the US National Science Foundation: NSF EAR 1446870.

497 **References**

- 498 Abatzoglou, J. T.: Development of gridded surface meteorological data for ecological applications and modelling,
499 Int. J. Climatol., doi:10.1002/joc.3413, 2013.
- 500
- 501 Bales, R. C., Hopmans, J. W., O'Geen, A. T., Meadows, M., Hartsough, P. C., Kirchner, P., Hunsaker, C. T. and
502 Beaudette, D.: Soil Moisture Response to Snowmelt and Rainfall in a Sierra Nevada Mixed-Conifer Forest, Vadose
503 Zo. J., 2011.
- 504
- 505 Barnhart, T. B., Molotch, N. P., Livneh, B., Harpold, A. A., Knowles, J. F. and Schneider, D.: Snowmelt rate
506 dictates streamflow, Geophys. Res. Lett., doi:10.1002/2016GL069690, 2016.
- 507
- 508 Berghuijs, W. R., Woods, R. A. and Hrachowitz, M.: A precipitation shift from snow towards rain leads to a
509 decrease in streamflow, Nat. Clim. Chang., doi:10.1038/nclimate2246, 2014.
- 510
- 511 Blankinship, J. C., Meadows, M. W., Lucas, R. G. and Hart, S. C.: Snowmelt timing alters shallow but not deep soil
512 moisture in the Sierra Nevada, Water Resour. Res., doi:10.1002/2013WR014541, 2014.
- 513
- 514 Brooks, P. D., Chorover, J., Fan, Y., Godsey, S. E., Maxwell, R. M., McNamara, J. P. and Tague, C.: Hydrological
515 partitioning in the critical zone: Recent advances and opportunities for developing transferable understanding of
516 water cycle dynamics, Water Resour. Res., doi:10.1002/2015WR017039, 2015.
- 517
- 518 Cho, H. and Olivera, F.: Effect of the spatial variability of land use, soil type, and precipitation on streamflows in
519 small watersheds, J. Am. Water Resour. Assoc., doi:10.1111/j.1752-1688.2009.00315.x, 2009.
- 520
- 521 Clow, D. W.: Changes in the timing of snowmelt and streamflow in Colorado: A response to recent warming, J.
522 Clim., doi:10.1175/2009JCLI2951.1, 2010.
- 523
- 524 Conner, L. G., Gill, R. A., and Belnap, J.: Soil moisture response to experimentally altered snowmelt timing is
525 mediated by soil, vegetation, and regional climate patterns. Ecohydrology, 9(6), 1006-1016, 2016.
- 526



- 527 Earman, S., Campbell, A. R., Phillips, F. M. and Newman, B. D.: Isotopic exchange between snow and atmospheric
528 water vapor: Estimation of the snowmelt component of groundwater recharge in the southwestern United States, *J.*
529 *Geophys. Res. Atmos.*, doi:10.1029/2005JD006470, 2006.
530
- 531 Eiriksson, D., Whitson, M., Luce, C. H., Marshall, H. P., Bradford, J., Benner, S. G., Black, T., Hetrick, H. and
532 Mcnamara, J. P.: An evaluation of the hydrologic relevance of lateral flow in snow at hillslope and catchment scales,
533 *Hydrol. Process.*, doi:10.1002/hyp.9666, 2013.
534
- 535 Flint, A. L., Flint, L. E. and Dettinger, M. D.: Modeling Soil Moisture Processes and Recharge under a Melting
536 Snowpack, *Vadose Zo. J.*, doi:10.2136/vzj2006.0135, 2008.
537
- 538 Furey, P. R., Kampf, S. K., Lanini, J. S. and Dozier, A. Q.: A Stochastic Conceptual Modeling Approach for
539 Examining the Effects of Climate Change on Streamflows in Mountain Basins, *J. Hydrometeorol.*, doi:10.1175/jhm-
540 d-11-037.1, 2012.
541
- 542 Gerten, D., Schaphoff, S., Haberlandt, U., Lucht, W. and Sitch, S.: Terrestrial vegetation and water balance -
543 Hydrological evaluation of a dynamic global vegetation model, *J. Hydrol.*, doi:10.1016/j.jhydrol.2003.09.029, 2004.
544
- 545 Gómez-Plaza, A., Martínez-Mena, M., Albaladejo, J. and Castillo, V. M.: Factors regulating spatial distribution of
546 soil water content in small semiarid catchments, *J. Hydrol.*, doi:10.1016/S0022-1694(01)00483-8, 2001.
547
- 548 Hammond, J. C., Saavedra, F. A. and Kampf, S. K.: How Does Snow Persistence Relate to Annual Streamflow in
549 Mountain Watersheds of the Western U.S. With Wet Maritime and Dry Continental Climates?, *Water Resour. Res.*,
550 doi:10.1002/2017WR021899, 2018.
551
- 552 Hammond, J. C., Saavedra, F. A. and Kampf, S. K.: Global snow zone maps and trends in snow persistence 2001–
553 2016, *Int. J. Climatol.*, doi:10.1002/joc.5674, 2018.
554
- 555 Harpold, A. A. and Kohler, M.: Potential for Changing Extreme Snowmelt and Rainfall Events in the Mountains of
556 the Western United States, *J. Geophys. Res. Atmos.*, doi:10.1002/2017JD027704, 2017.
557
- 558 Harpold, A. A.: Diverging sensitivity of soil water stress to changing snowmelt timing in the Western U.S., *Adv.*
559 *Water Resour.*, doi:10.1016/j.advwatres.2016.03.017, 2016.
560
- 561 Harpold, A. A. and Brooks, P. D.: Humidity determines snowpack ablation under a warming climate, *Proc. Natl.*
562 *Acad. Sci.*, doi:10.1073/pnas.1716789115, 2018.
563
- 564 Harpold, A. A. and Molotch, N. P.: Sensitivity of soil water availability to changing snowmelt timing in the western
565 U.S., *Geophys. Res. Lett.*, doi:10.1002/2015GL065855, 2015.
566
- 567 Harpold, A. A., Molotch, N. P., Musselman, K. N., Bales, R. C., Kirchner, P. B., Litvak, M. and Brooks, P. D.: Soil
568 moisture response to snowmelt timing in mixed-conifer subalpine forests, *Hydrol. Process.*, doi:10.1002/hyp.10400,
569 2015.
570
- 571 Hinckley, E. L. S., Ebel, B. A., Barnes, R. T., Anderson, R. S., Williams, M. W. and Anderson, S. P.: Aspect control
572 of water movement on hillslopes near the rain-snow transition of the Colorado Front Range, *Hydrol. Process.*,
573 doi:10.1002/hyp.9549, 2014.
574
- 575 Hu, J., Moore, D. J. P., Burns, S. P. and Monson, R.: Longer growing seasons lead to less carbon sequestration by a
576 subalpine forest, *Glob. Chang. Biol.*, doi:10.1111/j.1365-2486.2009.01967.x, 2010.
577
- 578 Hunsaker, C. T., Whitaker, T. W. and Bales, R. C.: Snowmelt Runoff and Water Yield Along Elevation and
579 Temperature Gradients in California's Southern Sierra Nevada, *J. Am. Water Resour. Assoc.*, doi:10.1111/j.1752-
580 1688.2012.00641.x, 2012.
581



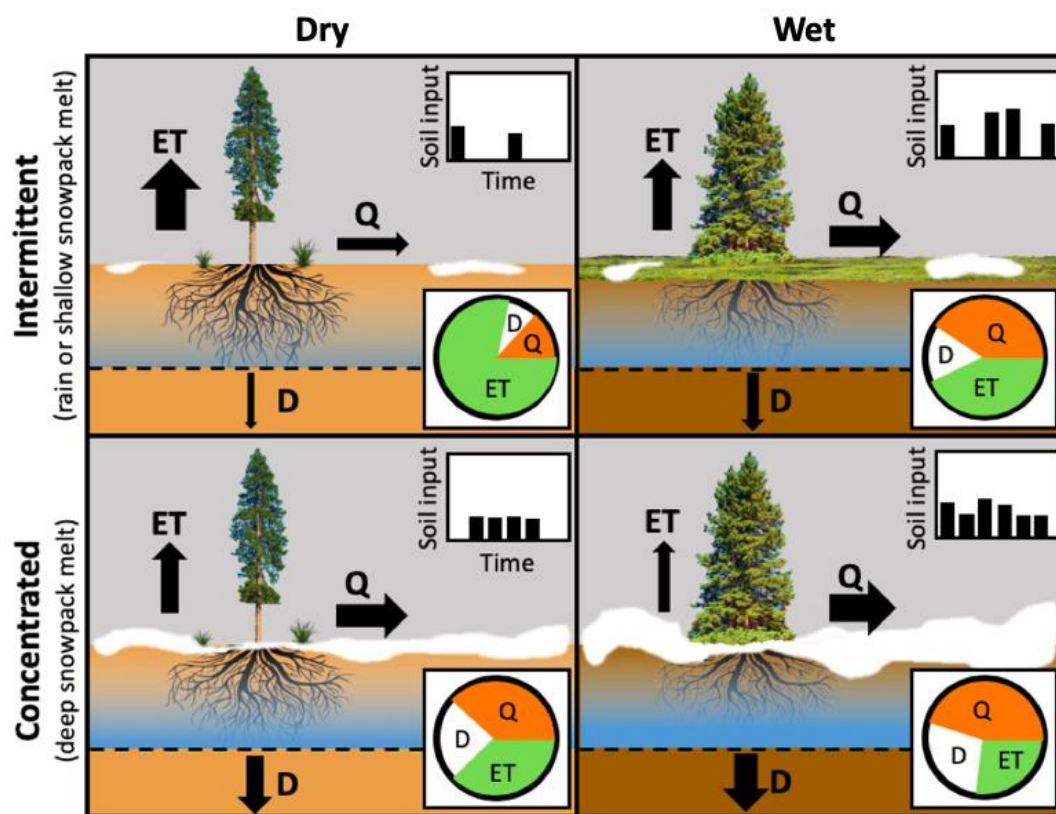
- 582 Jaynes, D. B., Ahmed, S. I., Kung, K.-J. S. and Kanwar, R. S.: Temporal Dynamics of Preferential Flow to a
583 Subsurface Drain, *Soil Sci. Soc. Am. J.*, doi:10.2136/sssaj2001.6551368x, 2010.
584
- 585 Jefferson, A. J.: Seasonal versus transient snow and the elevation dependence of climate sensitivity in maritime
586 mountainous regions, *Geophys. Res. Lett.*, doi:10.1029/2011GL048346, 2011.
587
- 588 Jepsen, S. M., Harmon, T. C., Meadows, M. W. and Hunsaker, C. T.: Hydrogeologic influence on changes in
589 snowmelt runoff with climate warming: Numerical experiments on a mid-elevation catchment in the Sierra Nevada,
590 USA, *J. Hydrol.*, doi:10.1016/j.jhydrol.2015.12.010, 2016.
591
- 592 Kaiser, K. and McGlynn B. L.: Nested scales of spatial and temporal variability of soil water content across a
593 semiarid montane catchment, *Water Resources Research*. DOI: 10.1029/2018WR022591, 2018.
594
- 595 Kampf, S., Markus, J., Heath, J. and Moore, C.: Snowmelt runoff and soil moisture dynamics on steep subalpine
596 hillslopes, *Hydrol. Process.*, doi:10.1002/hyp.10179, 2015.
597
- 598 Kormos, P. R., Marks, D., McNamara, J. P., Marshall, H. P., Winstral, A. and Flores, A. N.: Snow distribution, melt
599 and surface water inputs to the soil in the mountain rain-snow transition zone, *J. Hydrol.*,
600 doi:10.1016/j.jhydrol.2014.06.051, 2014.
601
- 602 Langston, A. L., Tucker, G. E., Anderson, R. S. and Anderson, S. P.: Evidence for climatic and hillslope-aspect
603 controls on vadose zone hydrology and implications for saprolite weathering, *Earth Surf. Process. Landforms*,
604 doi:10.1002/esp.3718, 2015.
605
- 606 Li, D., Wrzesien, M. L., Durand, M., Adam, J. and Lettenmaier, D. P.: How much runoff originates as snow in the
607 western United States, and how will that change in the future?, *Geophys. Res. Lett.*, doi:10.1002/2017GL073551,
608 2017.
609
- 610 Li, X., Jiang, F., Li, L. and Wang, G.: Spatial and temporal variability of precipitation concentration index,
611 concentration degree and concentration period Xinjiang, China, *Int. J. Climatol.*, doi:10.1002/joc.2181, 2011.
612
- 613 Litaor, M. I., Williams, M. and Seastedt, T. R.: Topographic controls on snow distribution, soil moisture, and
614 species diversity of herbaceous alpine Vegetation, *Netwot Ridge, Colorado*, *J. Geophys. Res. Biogeosciences*,
615 doi:10.1029/2007JG000419, 2008.
616
- 617 Liu, F., Parmenter, R., Brooks, P. D., Conklin, M. H. and Bales, R. C.: Seasonal and interannual variation of
618 streamflow pathways and biogeochemical implications in semi-arid, forested catchemnts in Valles Caldera, New
619 Mexico, *Ecohydrology*, doi:10.1002/eco.22, 2008.
620
- 621 Loik, M. E., Breshears, D. D., Lauenroth, W. K. and Belnap, J.: A multi-scale perspective of water pulses in dryland
622 ecosystems: Climatology and ecohydrology of the western USA, *Oecologia*, doi:10.1007/s00442-004-1570-y, 2004.
623
- 624 Lv, L.: Linking montane soil moisture measurements to evapotranspiration using inverse numerical modeling. *Utah*
625 *State University*, 2014.
626
- 627 M Foster, L., A Bearup, L., P Molotch, N., D Brooks, P. and M Maxwell, R.: Energy budget increases reduce mean
628 streamflow more than snow-rain transitions: Using integrated modeling to isolate climate change impacts on Rocky
629 Mountain hydrology, *Environ. Res. Lett.*, doi:10.1088/1748-9326/11/4/044015, 2016.
630
- 631 Markovich, K. H., Maxwell, R. M. and Fogg, G. E.: Hydrogeological response to climate change in alpine
632 hillslopes, *Hydrol. Process.*, doi:10.1002/hyp.10851, 2016.
633
- 634 Martin-Vide, J.: Spatial distribution of a daily precipitation concentration index in peninsular Spain, *Int. J. Climatol.*,
635 doi:10.1002/joc.1030, 2004.
636



- 637 McNamara, J. P., Chandler, D., Seyfried, M. and Achet, S.: Soil moisture states, lateral flow, and streamflow
638 generation in a semi-arid, snowmelt-driven catchment, *Hydrol. Process.*, doi:10.1002/hyp.5869, 2005.
639
- 640 Meixner, T., Manning, A. H., Stonestrom, D. A., Allen, D. M., Ajami, H., Blasch, K. W., Brookfield, A. E., Castro,
641 C. L., Clark, J. F., Gochis, D. J., Flint, A. L., Neff, K. L., Niraula, R., Rodell, M., Scanlon, B. R., Singha, K. and
642 Walvoord, M. A.: Implications of projected climate change for groundwater recharge in the western United States, *J.*
643 *Hydrol.*, doi:10.1016/j.jhydrol.2015.12.027, 2016.
644
- 645 Molotch, N. P., Brooks, P. D., Burns, S. P., Litvak, M., Monson, R. K., McConnell, J. R. and Musselman, K.:
646 Ecohydrological controls on snowmelt partitioning in mixed-conifer sub-alpine forests, *Ecohydrology*,
647 doi:10.1002/eco.48, 2009.
648
- 649 Moore, C., Kampf, S., Stone, B. and Richer, E.: A GIS-based method for defining snow zones: application to the
650 western United States, *Geocarto Int.*, doi:10.1080/10106049.2014.885089, 2015.
651
- 652 Musselman, K. N., Clark, M. P., Liu, C., Ikeda, K. and Rasmussen, R.: Slower snowmelt in a warmer world, *Nat.*
653 *Clim. Chang.*, doi:10.1038/nclimate3225, 2017.
654
- 655 National Water and Climate Center [NWCC]: Report Generator 2.0, [10/01/2003-09/30/2015]. Portland, Oregon,
656 USA, 2016.
657
- 658 Newman, B. D., Wilcox, B. P. and Graham, R. C.: Snowmelt-driven macropore flow and soil saturation in a
659 semiarid forest, *Hydrol. Process.*, doi:10.1002/hyp.5521, 2004.
660
- 661 Nolin, A. W. and Daly, C.: Mapping “At Risk” Snow in the Pacific Northwest, *J. Hydrometeorol.*,
662 doi:10.1175/jhm543.1, 2006.
663
- 664 Razieli, T., Bordi, I. and Pereira, L. S.: A precipitation-based regionalization for Western Iran and regional drought
665 variability, *Hydrol. Earth Syst. Sci.*, doi:10.5194/hess-12-1309-2008, 2008.
666
- 667 Regonda, S. K., Rajagopalan, B., Clark, M. and Pitlick, J.: Seasonal cycle shifts in hydroclimatology over the
668 western United States, *J. Clim.*, doi:10.1175/JCLI-3272.1, 2005.
669
- 670 Schaap, M. G., Leij, F. J. and Van Genuchten, M. T.: Rosetta: A computer program for estimating soil hydraulic
671 parameters with hierarchical pedotransfer functions, *J. Hydrol.*, doi:10.1016/S0022-1694(01)00466-8, 2001.
672
- 673 Scott, R. L., Shuttleworth, W. J., Keefer, T. O. and Warrick, A. W.: Modeling multiyear observations of soil
674 moisture recharge in the semiarid American Southwest, *Water Resour. Res.*, doi:10.1029/2000WR900116, 2000.
675
- 676 Šejna, M., Saito, H., Sakai, M. and Genuchten, M. T. van: The Hydrus-1D Software Package for Simulating the
677 Movement of Water, Heat, and Multiple Solutes in Variably Saturated Media., 2008.
678
- 679 Seyfried, M. S., Schwinning, S., Walvoord, M. A., Pockman, W. T., Newman, B. D., Jackson, R. B. and Phillips, F.
680 M.: Ecohydrological control of deep drainage in arid and semiarid regions, in *Ecology.*, 2005.
681
- 682 Seyfried, M. S., Grant, L. E., Marks, D., Winstral, A. and McNamara, J.: Simulated soil water storage effects on
683 streamflow generation in a mountainous snowmelt environment, Idaho, USA, *Hydrol. Process.*,
684 doi:10.1002/hyp.7211, 2009.
685
- 686 Šimůnek, J., M. Šejna, and van Genuchten M.: The HYDRUS-1D software package for simulating the one-
687 dimensional movement of water, heat, and multiple solutes in variably saturated media. Version 1.0. IGWMC-TPS-
688 70. Golden, Colo.: Colorado School of Mines, International Ground Water Modeling Center, 1998.
689
- 690 Slater, A. G., Lawrence, D. M. and Koven, C. D.: Process-level model evaluation: A snow and heat transfer metric,
691 *Cryosphere*, doi:10.5194/tc-11-989-2017, 2017.
692

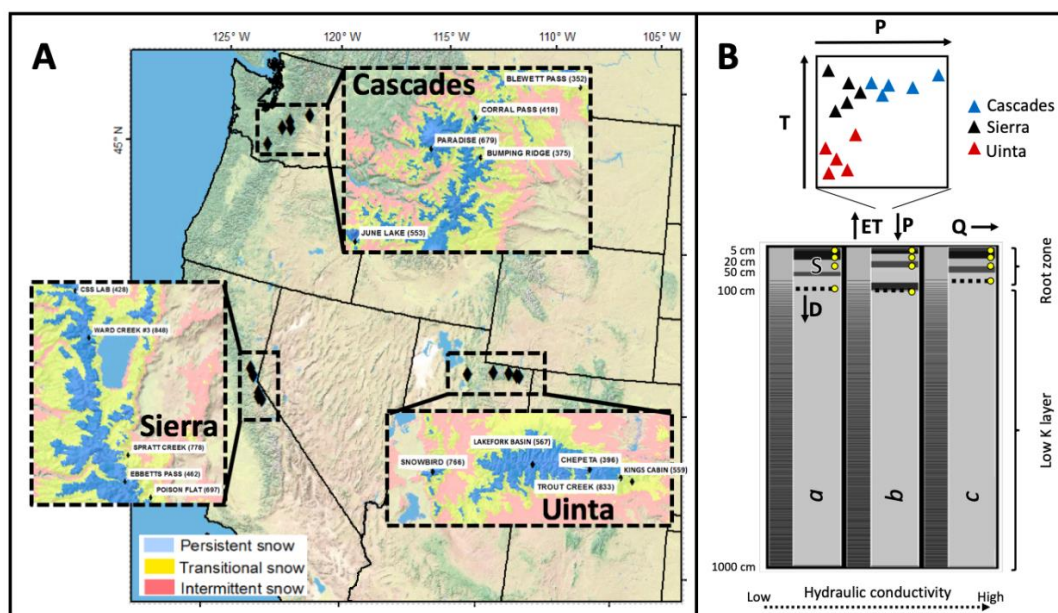


- 693 Smith, T. J., Mcnamara, J. P., Flores, A. N., Gribb, M. M., Aishlin, P. S. and Benner, S. G.: Small soil storage
694 capacity limits benefit of winter snowpack to upland vegetation, *Hydrol. Process.*, doi:10.1002/hyp.8340, 2011.
695
- 696 Stewart, I. T., Cayan, D. R. and Dettinger, M. D.: Changes toward earlier streamflow timing across western North
697 America, *J. Clim.*, doi:10.1175/JCLI3321.1, 2005.
698
- 699 Sukhija, B. S., Reddy, D. V., Nagabhushanam, P. and Hussain, S.: Recharge processes: Piston flow vs preferential
700 flow in semi-arid aquifers of India, *Hydrogeol. J.*, doi:10.1007/s10040-002-0243-3, 2003.
701
- 702 Tague, C. and Peng, H.: The sensitivity of forest water use to the timing of precipitation and snowmelt recharge in
703 the California Sierra: Implications for a warming climate, *J. Geophys. Res. Biogeosciences*, doi:10.1002/jgrg.20073,
704 2013.
705
- 706 Webb, R. W., Fassnacht, S. R. and Gooseff, M. N.: Wetting and Drying Variability of the Shallow Subsurface
707 Beneath a Snowpack in California's Southern Sierra Nevada, *Vadose Zo. J.*, doi:10.2136/vzj2014.12.0182, 2015.
708
- 709 Webb, R. W., Fassnacht, S. R. and Gooseff, M. N.: Defining the Diurnal Pattern of Snowmelt Using a Beta
710 Distribution Function, *J. Am. Water Resour. Assoc.*, doi:10.1111/1752-1688.12522, 2017.
711
- 712 Webb, R. W., Fassnacht, S. R. and Gooseff, M. N.: Hydrologic flow path development varies by aspect during
713 spring snowmelt in complex subalpine terrain, *Cryosphere*, doi:10.5194/tc-12-287-2018, 2018.
714
- 715 Williams, C. J., McNamara, J. P. and Chandler, D. G.: Controls on the temporal and spatial variability of soil
716 moisture in a mountainous landscape: The signature of snow and complex terrain, *Hydrol. Earth Syst. Sci.*,
717 doi:10.5194/hess-13-1325-2009, 2009.
718
- 719 Wood, W. W., Rainwater, K. A. and Thompson, D. B.: Quantifying Macropore Recharge: Examples from a Semi-
720 Arid Area, *Ground Water*, doi:10.1111/j.1745-6584.1997.tb00182.x, 2005.
721
- 722 Yan, H., Sun, N., Wigmosta, M., Skaggs, R., Hou, Z. and Leung, R.: Next-Generation Intensity-Duration-Frequency
723 Curves for Hydrologic Design in Snow-Dominated Environments, *Water Resour. Res.*,
724 doi:10.1002/2017WR021290, 2018.
725
- 726 Zeng, X., Zeng, X., Shen, S. S. P., Dickinson, R. E. and Zeng, Q. C.: Vegetation-soil water interaction within a
727 dynamical ecosystem model of grassland in semi-arid areas, *Tellus, Ser. B Chem. Phys. Meteorol.*,
728 doi:10.1111/j.1600-0889.2005.00151.x, 2005.
729
730
731
732



733

734 **Figure 1. Conceptual illustration of study hypotheses indicating the importance of concentrated snowmelt**
 735 **input (bottom panels) versus intermittent input (top panels) for runoff generation. The wet climate (right-**
 736 **hand panels) generates more runoff (Q) and deep drainage (D) and less evapotranspiration (ET) compared to**
 737 **the dry climate (left-hand panels). In both climates, concentrated input can increase both Q and D because it**
 738 **is more likely to allow soil saturation than intermittent input, which allows ET during periods of drying. The**
 739 **concentrated input from snowmelt leads to greater increases in Q and D in the dry climate than in the wet**
 740 **climate because snowmelt is the most likely cause of soil saturation in dry climates.**
 741



742

743

744

745

746

747

748

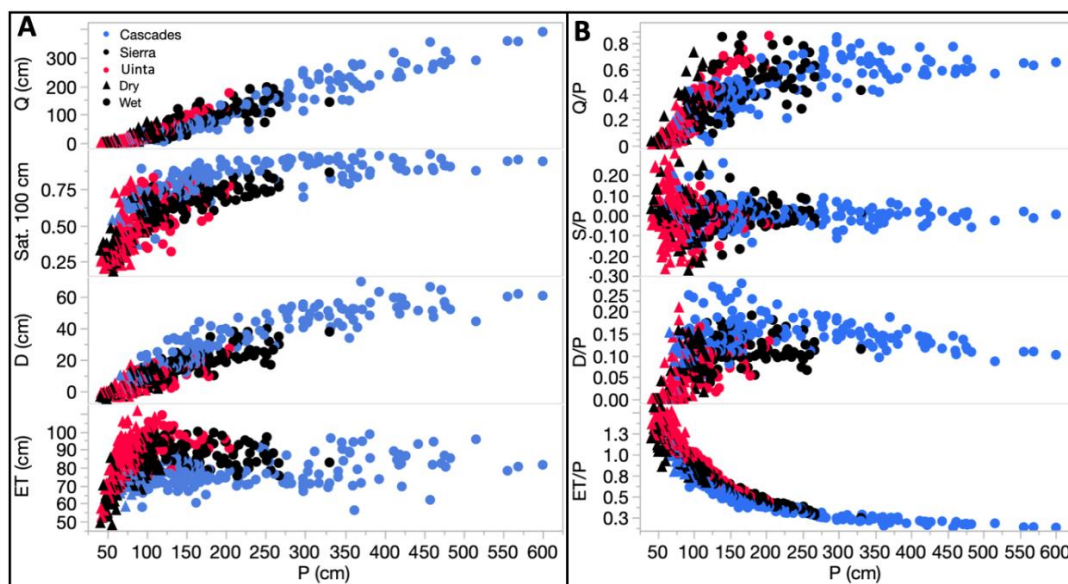
749

750

751

752

Figure 2. (A) SNOTEL sites utilized for climate scenarios in this study with insets displaying snow zones classified by mean annual snow persistence (Moore et al., 2015). (B) Modeling domain layout with yellow points showing 5, 20 and 50 cm depths where volumetric water content time series were used for model calibration. Deepest yellow point is the depth where time series were extracted to calculate deep saturation. Symbols in the graph above the discretized soil profile represent the range of climate scenarios used plotted by mean annual precipitation (P) and mean annual temperature (T), and the three soil profiles below represent the soil parameter sets labeled with italicized capital letters (*a*) loam (*b*) sandy clay loam (*c*) sandy loam. Different layers in each soil profile are represented as shades of gray.

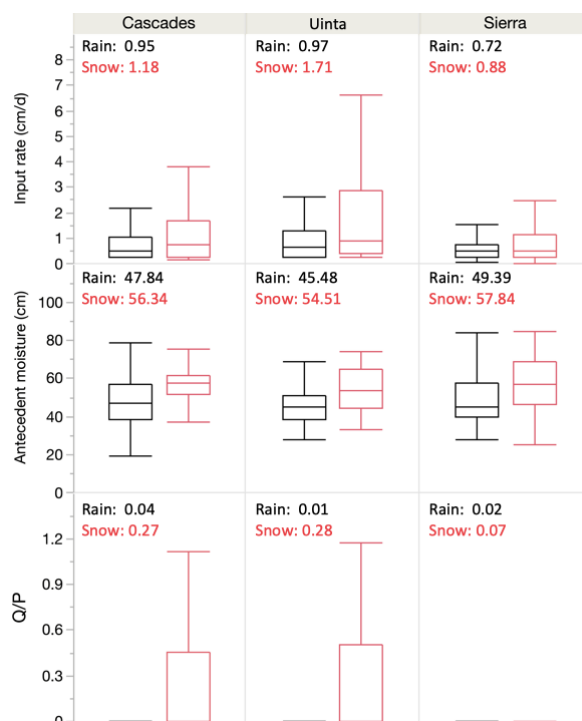


753

754 **Figure 3. A) Annual runoff (Q), mean saturation at 100 cm depth (Sat100), deep drainage (D) and**
755 **evapotranspiration (ET) vs annual precipitation (P) classified by region and climate type. B) Q/P, ΔS/P, D/P**
756 **and ET/P vs P classified by region and climate type. Dry sites P/PET ≤1, Wet P/PET >1. Data from historical**
757 **input scenarios for soil profile 1056, loam.**

758

759



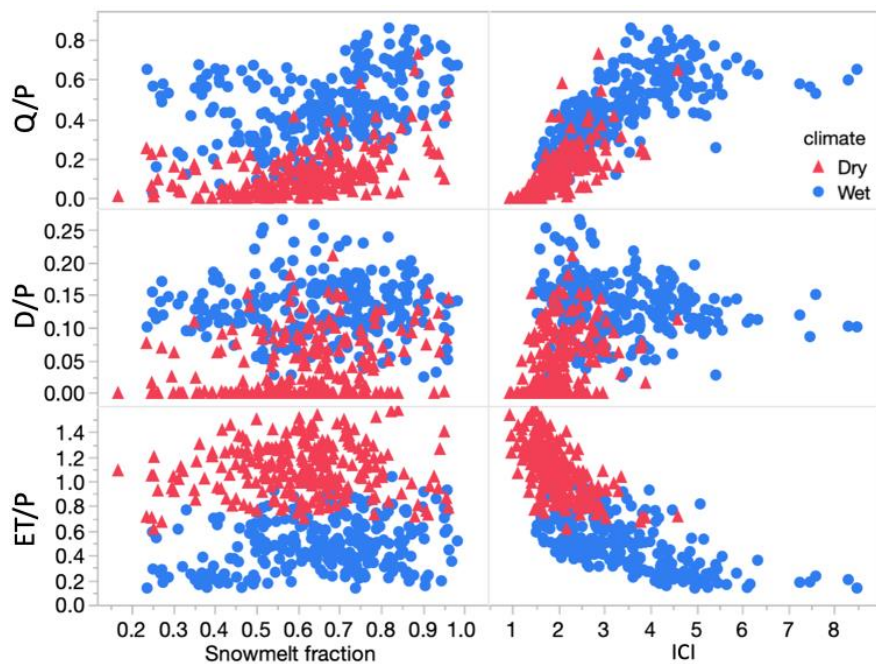
760

761 **Figure 4.** Boxplots of event input rate (cm/d) (top), antecedent soil moisture storage (S, cm) (middle) and
 762 event runoff ratio (Q/P, bottom) by region and event type (rain black, snowmelt red). Text in each subplot
 763 gives mean values. All ANOVA comparisons between values for rain and snowmelt have p-values <0.0001.
 764 Results from historical simulations on loam profile.

765

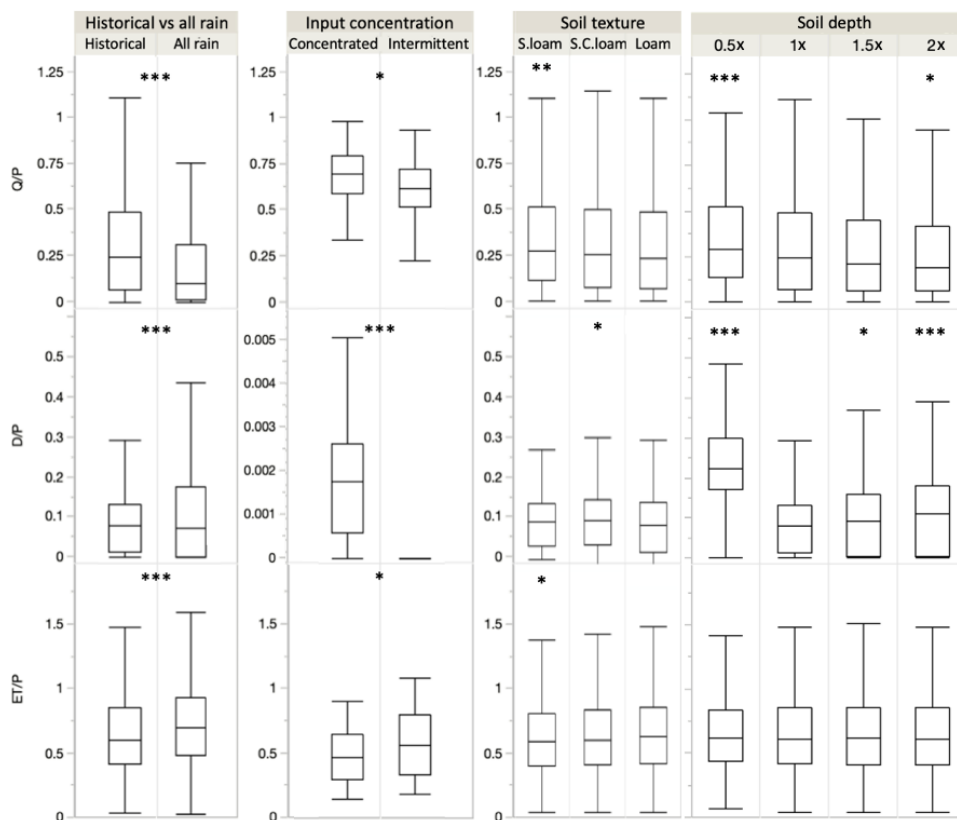
766

767



768

769 **Figure 5. Ratio of runoff (Q), deep drainage (D) and evapotranspiration (ET) to input (P) vs. snowmelt**
770 **fraction of input and input concentration index (ICI) at the annual time scale. Data from historical**
771 **simulations on loam profile. Dry sites $P/PET < 1$, Wet $P/PET > 1$.**
772

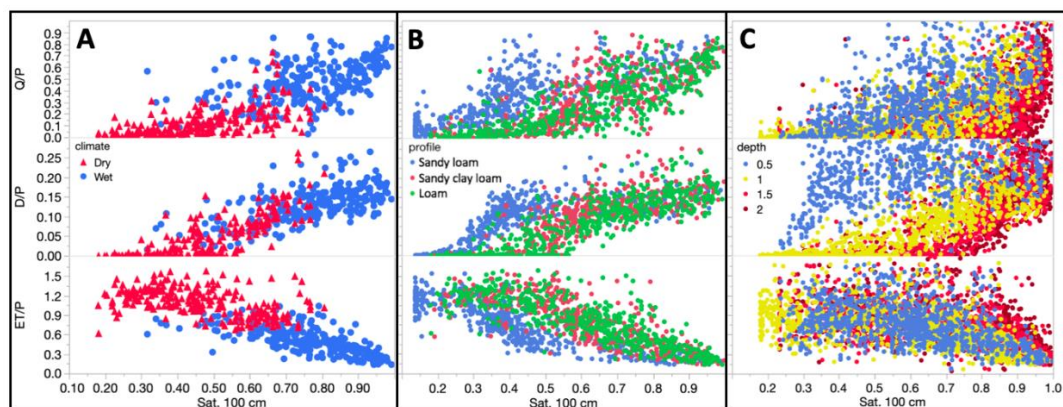


773

774 **Figure 6. Boxplots of Q/P, D/P and ET/P for four different experiments: historical vs all rain input on loam**
 775 **soil and constant 1x depth, intermittent vs concentrated input on loam soil and constant 1x depth, different**
 776 **soil textures with constant 1x depth, and different soil depths all with loam soil texture. Asterisks denote**
 777 **significance of ANOVA tests between groupings. P-value of ANOVA, *<0.5, **<0.01, ***<0.001. Boxplots**
 778 **correspond with values in Table 3. Soil texture and soil depth scenarios are compared to 1x depth and loam**
 779 **texture profile for ANOVAs.**

780

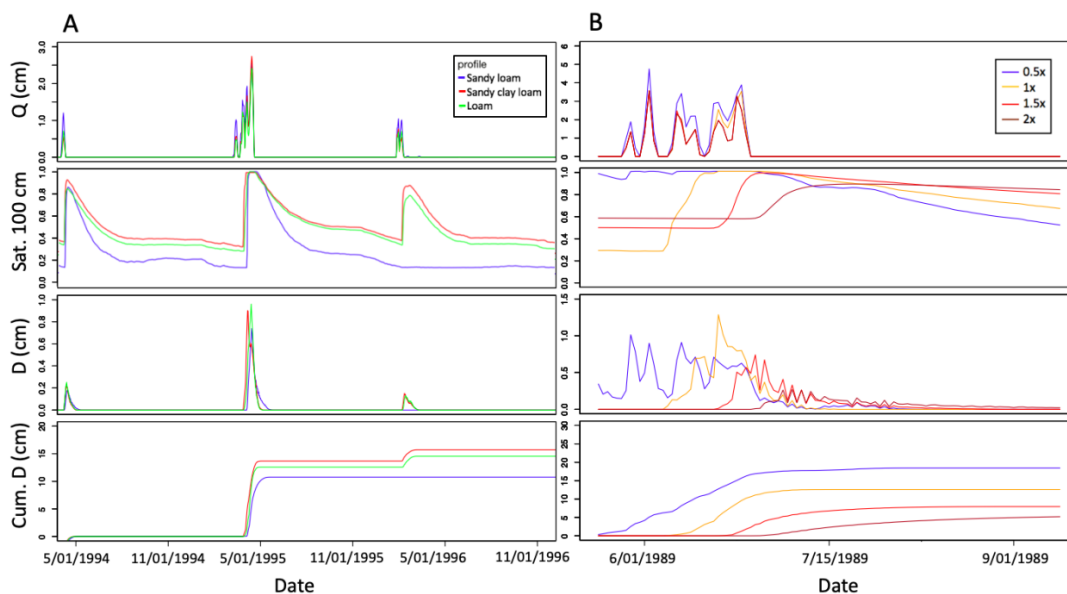
781



782

783 **Figure 7. A) Annual surface runoff (Q), deep drainage (D) and evapotranspiration (ET) as a fraction of**
 784 **annual precipitation (P) vs annual mean saturation at 100 cm depth (Sat100) and classified by climate on**
 785 **the loam profile, Dry sites P/PET <=1, Wet P/PET >1. B) The same variables displayed in A but classified by**
 786 **soil texture on three different soil profiles. C) The same variables in A but classified by root zone depth on**
 787 **four different profiles of differing root zone depth. All simulations use historical input.**

788



789

790 **Figure 8. (A) daily time series of runoff (Q), saturation at 100 cm depth (Sat100), deep drainage (D), and**
 791 **cumulative deep drainage for SNOTEL site 698 input on SNOTEL site 515 (sandy loam), 1049 (sandy clay**
 792 **loam) and 1056 (loam) profile. (B) daily series for the same variables plotted for four depth scenarios 0.5x, 1x**
 793 **1.5x and 2x original rooting zone depth.**



Table 1. SNOTEL station properties including the start and end of data records, site elevation, and mean annual climatic characteristics: precipitation (P), temperature (T), snow persistence (SP, %), and aridity index (P/PET).

SNOTEL ID	Region	State	Start	End	Elevation (m)	P (cm)	T (C)	SP	P/PET
352	Cascades	WA	1981	2015	1292	90	6.3	54	0.8
553	Cascades	WA	1982	2015	1049	433	6.9	65	4.4
375	Cascades	WA	1978	2015	1405	146	4.9	69	1.8
679	Cascades	WA	1980	2015	1564	263	4.8	77	4.9
418	Cascades	WA	1981	2015	1768	158	3.6	83	1.9
778	Sierra	CA	1980	2015	1864	69	8.0	53	0.7
697	Sierra	CA	1980	2015	2358	98	3.8	63	0.6
428	Sierra	CA	1981	2015	2089	180	6.0	72	1.3
848	Sierra	CA	1978	2015	2028	197	5.9	74	1.3
462	Sierra	CA	1978	2015	2672	142	4.0	78	1
559	Uinta	UT	1979	2015	2659	74	1.4	60	0.6
833	Uinta	UT	1979	2015	2901	70	1.5	69	0.7
396	Uinta	UT	1981	2015	3228	81	-0.1	76	0.9
567	Uinta	UT	1980	2015	3342	98	0.0	86	0.9
766	Uinta	UT	1989	2015	2938	157	3.2	87	1.3



Table 2. Soil profile properties derived from NRCS pedon reports and ROSETTA (Ros.) neural network. Columns are SNOTEL site, soil profile horizon, depth range of horizon, rock percent of sample volume, organic carbon percent of sample volume, sand percent of sample weight, silt percent of sample weight, clay percent of sample weight, Db_{33} bulk density of soil sample desorbed to 33kPa, Θ_{33} volumetric water content at field capacity, Θ_{1500} volumetric water content at wilting point, soil texture, residual volumetric water content Θ_r , saturated volumetric water content Θ_s , pore size distribution parameter α , and K_s saturated hydraulic conductivity. The lowest horizon K_s value was calibrated. Soil textures abbreviated as follows: sandy loam (SL), sand (S), loamy sand (LS), sandy clay loam (SCL), loam (L). SNOTEL 515, Harts Pass, WA, SNOTEL 1049, Forestdale Creek, CA, SNOTEL 1056, Lightning Ridge, UT.

Site	Hor.	Depth (cm)	rock % vol	organic C % vol	sand % wt	silt % wt	clay % wt	Db_{33} g cm^{-3}	Θ_{33}	Θ_{1500}	Text.	Ros. Θ_r	Ros. Θ_s	Ros. α (1/cm)	Ros. K_s (cm/d)
515	A1	0-15	9	9	53.5	35.6	10.9	0.63	0.41	0.14	SL	0.06	0.62	0.009	17.4
515	A2	13-38	8	8	57.6	35.3	7.1	0.64	0.47	0.14	SL	0.05	0.60	0.011	20.5
515	2Bw1	38-61	27	3	73.1	22.1	4.8	0.86	0.3	0.08	SL	0.04	0.55	0.032	15.1
515	2Bw2	61-81	55	1	81	11	8	1.46	0.16	0.09	LS	0.05	0.40	0.036	5.49
515	Cd	81-106	7	1	91.3	4.1	4.6	1.52	0.14	0.05	S	0.05	0.38	0.033	17.4
515	Cd	106-1000	7	1	91.3	4.1	4.6	1.52	0.14	0.05	S	0.05	0.38	0.033	1.74
1049	A	0-9	10	7	52.6	25.2	22.2	0.94	0.40	0.14	SCL	0.08	0.55	0.014	5.17
1049	Bt1	9-20	14	2	48.6	25.4	26	1.13	0.30	0.14	SCL	0.08	0.50	0.014	2.13
1049	Bt2	20-43	14	1	52.9	23.8	23.3	1.24	0.32	0.12	SCL	0.07	0.47	0.016	1.74
1049	Bt3	43-63	21	1	53.4	24	22.6	1.19	0.33	0.13	SCL	0.07	0.48	0.015	2.18
1049	Bt4	63-77	19	1	55.5	25.9	18.6	1.39	0.32	0.12	SL	0.06	0.42	0.017	1.22
1049	Bt5	77-110	11	0	52.4	30.2	17.4	1.21	0.39	0.13	SL	0.06	0.45	0.013	2.22
1049	Bt5	110-1000	11	0	52.4	30.2	17.4	1.21	0.39	0.13	SL	0.06	0.45	0.013	0.22
1056	A	0-10	11	3	36.1	48.8	15.1	1.17	0.30	0.12	L	0.06	0.44	0.010	2.41
1056	A	10-38	7	2	35.3	49.5	15.2	1.27	0.28	0.11	L	0.06	0.41	0.006	1.47
1056	Bt1	38-76	6	2	36	48.6	15.4	1.25	0.30	0.10	L	0.06	0.42	0.006	1.59
1056	Bt2	76-89	16	1	39.3	46	14.7	1.26	0.34	0.09	L	0.06	0.41	0.007	1.54
1056	2B	89-127	6	2	36.3	48.2	15.5	1.18	0.24	0.09	L	0.06	0.44	0.006	2.23
1056	2B	127-1000	6	2	36.3	48.2	15.5	1.18	0.24	0.09	L	0.06	0.44	0.006	0.22



Table 3. Mean values of unitless response variables Q/P, D/P, and ET/P compared by climate type for four hypothetical scenarios: (1) historical vs all rain input, (2) intermittent vs concentrated input, (3) historical input on sandy loam, sandy clay loam, and loam profiles, (4) historical input on 0.5x, 1x, 1.5x and 2x original rooting zone depth. Dry sites P/PET ≤ 1 , Wet P/PET > 1 . All scenarios in the table besides those explicitly altering soil texture use the loam profile (1056). Asterisks denote the significance of ANOVA tests between groupings of simulations and arrows show the direction of change relative to the base scenario: historical input on 1x depth profile with loam texture. P-value of ANOVA, * < 0.5 , ** < 0.01 , * < 0.001 . Boxplots correspond with values in Table 3.**



Experiment	Scenario	Climate	Q/P	D/P	ET/P	
Historical vs. all rain	Historical	All	0.31	0.09	0.66	
		Wet	0.44	0.12	0.51	
		Dry	0.13	0.03	0.83	
	All rain	All	0.19↓***	0.12↑	0.73↑**	
		Wet	0.28↓***	0.14↑*	0.55↑	
		Dry	0.04↓***	0.01↓***	0.95↑***	
Intermittent vs. concentrated ²	Intermittent	All	0.59	0.00	0.58	
		Wet	0.64	0.00	0.34	
		Dry	0.54	0.00	0.80	
	Concentrated	All	0.68↑*	0.002↑***	0.48↓*	
		Wet	0.68↑	0.002↑***	0.28↓*	
		Dry	0.68↑*	0.002↑***	0.66↓**	
Soil texture	Loam (L)	All	0.31	0.09	0.66	
		Wet	0.44	0.12	0.51	
		Dry	0.13	0.03	0.83	
	Sandy loam (SL)	All	0.35**↑	0.09	0.63↓*	
		Wet	0.05↓	0.13↑	0.51↓	
		Dry	0.19↑*	0.05↑	1.01↓* ¹	
	Sandy clay loam (SCL)	All	0.32↑	0.10↑*	0.65↓	
		Wet	0.48↑	0.14↑	0.52↑	
		Dry	0.14↑	0.06↑	1.08↓ ¹	
	Soil depth	0.5x	All	0.35↑***	0.25↑***	0.67↑
			Wet	0.54↑***	0.28↑***	0.53↑*
			Dry	0.17↑**	0.22↑***	0.80↓*
1x		All	0.31	0.09	0.66	
		Wet	0.44	0.12	0.51	
		Dry	0.13	0.03	0.83	
1.5x		All	0.29↓	0.10↑*	0.67↑	
		Wet	0.46↑	0.16↑*	0.51	
		Dry	0.09↓	0.03	0.84↑	
2x		All	0.27↓*	0.11↑***	0.66	
		Wet	0.44	0.18↑***	0.51	
		Dry	0.09↓	0.04↑	0.84↑	

¹Values of ET/P >1 indicate root uptake from soil storage for years with low input (Figure S5).

²For a dry site (375) and a wet site (559). Intermittent simulations have annual total input separated into four five-day periods, whereas concentrated input simulations have all input in twenty-day period of high magnitude.